A01-31139

AIAA 2001–2549

Mesh Adaptation using Different Error Indicators for the Euler Equations

Xu Dong Zhang, Marie-Gabrielle Vallet, Julien Dompierre, Paul Labbé, Dominique Pelletier, Jean-Yves Trépanier, Ricardo Camarero,
Centre de recherche en calcul appliqué (CERCA)
5160, boul. Décarie, bureau 400,
Montréal, Québec, H3X 2H9, Canada.
Jason V. Lassaline, Luis M. Manzano, David W. Zingg
University of Toronto Institute for Aerospace Studies (UTIAS)
4925, Dufferin Street,
Toronto, Ontario, M3H 5T6, Canada.

15th AIAA Computational Fluid Dynamics Conference
June 11–14, 2001 / Anaheim, CA

Mesh Adaptation using Different Error Indicators for the Euler Equations

Xu Dong Zhang,*
Marie-Gabrielle Vallet,*
Julien Dompierre,*
Paul Labbé,*
Dominique Pelletier,†
Jean-Yves Trépanier,†
Ricardo Camarero,†
Centre de recherche en calcul appliqué (CERCA)
5160, boul. Décarie, bureau 400,
Montréal, Québec, H3X 2H9, Canada.
Jason V. Lassaline,‡
Luis M. Manzano,§
David W. Zingg†
University of Toronto Institute for Aerospace Studies (UTIAS)
4925, Dufferin Street,
Toronto, Ontario, M3H 5T6, Canada.

Abstract

This paper investigates the efficiency of mesh adaptation methods to control the error in the solution of one- and two-dimensional Euler equations. Two types of error indicators are compared: error indicators based on solution reconstruction and indicators based on evaluation of the partial differential equations. Numerical tests in one dimension confirm that a residual error indicator is a most efficient way to reduce both the error and the residual for of subsonic flows. In the case of transonic flows, however, the use of a residual error indicator is not locally effective for the sonic region. Some results concerning solution error indicators are extended to two-dimensional cases, but further work is required to develop an effective residual error indicator for the two-dimensional Euler equations.

1. Introduction

MESH adaptation is one of the most attractive strategy to obtain highly accurate solutions in computational fluid dynamics (CFD). The generation of such adapted meshes is usually guided by a proper error indicator. The ultimate goal of mesh adaptation is to minimize and control the discretization error. To achieve this goal, a reliable *a posteriori* error indicator is a basic requirement.

Different error indicators have been proposed and used for the Euler and Navier-Stokes equations. A well-known error estimation for engineering applications has been proposed by Zienkiewicz and Zhu[1,2] in which local gradient recovery techniques are used to obtain a higher order projection of the solution. The difference between the solution and higher order projection is used as an estimate of the error. Another error estimation, proposed by Roache,[3] uses the classical Richardson extrapolation technique and involves the solutions obtained on a set of meshes of different size. The extrapolated difference between two solutions obtained on different meshes can assess the solution error. An alternate approach has been proposed by Zhang *et al.*[4] to make error estimation more relevant by accounting for the error transport in convection dominated problems. This approach is based on solving a linearized equation system for the solution error.

However, for hyperbolic equations such as those encountered in aerodynamic applications, one can argue that mesh adaptation only guided by the solution error may not be optimal. More efficient error control should involve minimizing the error from the discretization of the partial differential equations (PDEs), which

*Research Professional
†Professor
‡Graduate Student
§Research Engineer

can be measured through their corresponding residuals.[4,5] Efforts at trying to control the error by mesh adaptation based on residual have shown some advantages for one-dimensional problems.[6,7] A weak measure of the residual using a dual-graph norm has been applied for two-dimensional compressible Euler equations[8] and has demonstrated impressive results for mesh adaptation.

In this paper, mesh adaptation driven by different error indicators will be investigated. The objective is to compare their performance and to assess their efficiency for error control through mesh adaptation. Results on quasi-one-dimensional problems and on two-dimensional flows over an NACA0012 airfoil are presented at the end of this paper.

The paper is organized as follows. The governing equations are first given, different error indicators are described, and the mesh adaptation strategy is discussed. Numerical examples include one-dimensional and two-dimensional tests, subsonic and transonic.

2. Governing Equations and Numerical Algorithms

The Euler equations governing the two-dimensional flow of an inviscid and compressible fluid can be written in a compact form as

$$\frac{\partial \mathbf{Q}}{\partial t} + \nabla \cdot \mathcal{F} = 0, \tag{1}$$

where $\mathbf{Q}$ represents a vector of the conserved unknown variables and $\mathcal{F}$ the flux matrix-functions of $\mathbf{Q}$ with the following expressions

$$\mathbf{Q} = \begin{pmatrix} \rho \\ \rho u \\ \rho v \\ \rho e \end{pmatrix}, \quad \mathcal{F} = \begin{pmatrix} \rho u & \rho v \\ \rho u^2 + p & \rho uv \\ \rho uv & \rho v^2 + p \\ (\rho e + p)u & (\rho e + p)v \end{pmatrix},$$

in which ρ is the density, p the static pressure, $\mathbf{u} = (u, v)$ the velocity vector, ρe the total energy which is related to other variables by the following equation

$$\rho e = p/(\gamma - 1) + \rho q^2/2,$$

where γ is the ratio of specific heat capacities of the fluid and $q = \|\mathbf{u}\|$ is the magnitude of the velocity vector.

A weak form of Eq. (1) can be written as an integral equation system

$$\frac{\partial}{\partial t}\int_V \mathbf{Q}\, dv + \oint_{\partial V} \mathcal{F} \cdot \mathbf{n}\, ds = 0, \tag{2}$$

where $\mathbf{n}$ is the outward normal unit vector of a control volume V.

The solutions are computed using a flow solver developed at the University of Toronto Institute for Aerospace Studies (UTIAS)[1] as part of the HURRICANE research project, a joint research project between UTIAS, École Polytechnique de Montréal, CERCA and Bombardier Aerospace Inc. The conserved flow variables are solved by a multi-stage Runge-Kutta time-marching method and a finite volume spatial discretization with scalar or matrix dissipations. To speed up the solution convergence, an agglomeration multigrid technique with directional coarsening has been used. The details about the numerical algorithms used in the solver can be found in Lassaline and Zingg.[9]

3. Error Estimation and its Control

Global control of the solution error is generally termed *a priori* error estimate for a given numerical method. It ensures the convergence of the method when the mesh size tends to zero, a basic requirement for any numerical method. The global error estimation may be expressed as

$$\|u - u_h\|_{W,\Omega} = \mathcal{O}(h^\alpha), \quad \text{with } h = \max_{K \in \mathcal{P}_h}(h_K) \tag{3}$$

where $\|\cdot\|_{W,\Omega}$ is a proper norm over the whole domain of interest Ω in a Sobolev space W, $\mathcal{P}_h$ is the mesh partition established over $\overline{\Omega}$, and h_K represents the size of element $K \in \mathcal{P}_h$. The superscript $\alpha > 0$ represents the convergence rate for the numerical method. For elliptic equations and finite element methods, this type of error estimation with $W = H^1(\Omega)$ can be found in Ciarlet.[10] For hyperbolic equations and finite volume methods, similar results with the L_2-norm were given in Morton and Suli.[11] It is evident that the order of convergence depends on both the problem and the method. It is also strongly dependent on the norm used to measure the error.

The exact error is rarely available for most problems of interest. To control the true error globally, one relies on a specific error estimator and tries to control the estimated error instead. However, the purpose of using adaptive techniques to control the estimated error is to ultimately allow us to control the true error. This requires that the estimated error must have a behavior similar to the true error. The efficiency index defined by

$$\theta = \frac{\|e\|}{\|u - u_h\|}$$

is a measure for the reliability and the efficiency for an estimated error $\|e\|$. The property of asymptotic exactness ($\theta \longrightarrow 1$ when $h \longrightarrow 0$) may not be a necessary

[1] See http://oddjob.utias.utoronto.ca/hurricane.

condition for mesh adaptation. A reasonable constant difference should be good enough to guide the adaptation and control the true error as well. Lack of proper asymptotic behavior ($\theta \longrightarrow 0$ or $\theta \longrightarrow \infty$ when $h \longrightarrow 0$) may mislead the mesh adaptation and the error control.

3.1. Solution Reconstruction

One widely used error estimator is based on solution reconstruction or solution recovery techniques.[1,12,13] The idea is as follows: one expects to estimate the solution error $e = u - u_h$ without knowing the exact solution u, where u is a chosen variable such as density ρ. The exact solution u is approximated by a higher order reconstruction of u_h. This reconstruction is usually noted u^*. The difference between the reconstruction and the numerical solution can be used as an error estimator, which can be written as $e = u^* - u_h$.

The order of the scheme generally represents the order of interpolation for u_h. For piecewise linear approximation of u_h (second-order scheme), the error is simply the departure of the quadratic terms of the Taylor expansion which form the Hessian matrix of second-order derivatives.

The advantage of using the Hessian matrix as estimation for the error is that it is frequently used to provide all the information needed for anisotropic mesh adaptation.[14,15] This type of error estimation is an analog of the approximation error of finite element methods. Only the local variation of the variables is used. It has been demonstrated to be efficient for elliptic equations. For hyperbolic cases, its efficiency has not been proven specially across discontinuities. It does not account for the transport of the error, either.

3.2. Residual of PDEs

Following Babuška and Rheinboldt,[16] some efforts have been focused on explicit residual type error estimators.[17,18] Consider the partial differential equation

$$\mathcal{L}u = f \tag{4}$$

over a given domain Ω for a linear differential operator $\mathcal{L}$. Let u_h denote the numerical approximation to the exact solution u, and $r = \mathcal{L}u_h - f$ denote the corresponding residual. The equation for the error $e = u - u_h$ can be written as

$$\mathcal{L}e = r \tag{5}$$

and one has the following explicit estimate of the error

$$||e||_{(1)} \leq C||r||_{(2)} \tag{6}$$

with suitable norms $||\cdot||_{(1)}$, $||\cdot||_{(2)}$ and a constant C. For non-linear equations, a constant C may not exist making the analysis more difficult. From traditional concern, the L_2-norm is the natural choice. However, as demonstrated in Sonar[17] and Mackenzie *et al*,[18] $||r||_{L_2} = \mathcal{O}(h^{-1/2})$, so that it is uncontrollable for one-dimensional hyperbolic problems in the presence of a shock. Detailed verification of different norms for one-dimensional problems can be found in Zhang *et al.*[6] To be able to control the residual error, weaker measures[17] of the residual have been used over each element K. For example,

$$\begin{aligned} e_{L_2} &= ||hr||_{L_2(K)}, \\ e_{H^{-1}} &= ||r||_{H^{-1}(K)}, \end{aligned} \tag{7}$$

have been proposed in Sonar.[17] Since the norm $||\cdot||_{H^{-1}(K)}$ is practically uncomputable, an approximation[17,18] was used to evaluate its value for each element K by

$$||r||_{H^{-1}(K)} \approx \max_i \frac{\left|\int_K r\phi_i \, dx\right|}{||\phi_i||_{H^1(K)}}$$

where $\phi_i, i = 1, 2, ..., n_i$ are some properly chosen functions in $H_0^1(K)$. With this approximation, the two weak norms given in Eq. (7) are typically equivalent.[19]

4. Mesh Adaptation Strategy

The mesh adaptation strategy will be to equidistribute the estimated error. For one-dimensional problems, a mesh can be computed that satisfies exactly a size specification map. For two-dimensional problems, the mesh adaptation strategy becomes more sophisticated and more complex. The mesh is modified iteratively so as to converge to the target size specification map.

4.1. One-Dimensional Problems

The goal is to compute a mesh that equidistributes the estimated error for a given number of elements. The local error estimator denoted by $||e_i||$ is computed in each element. Here $||\cdot||$ represents an appropriately chosen norm. The global error on the mesh is defined by $||e|| = \sum_i ||e_i||$. The new mesh will have the same global error, but the local error estimator should be equidistributed over all the elements of the new mesh. All the elements of the new mesh will therefor have the same amount of error. For a fixed number of elements N, the target equidistributed error is computed by:

$$||e|| = \sum_i ||e_i|| = N||\bar{e}||. \tag{8}$$

It is assumed that $||e_i|| \propto h_i^p$, where h_i is the current mesh size and p the convergence rate.[20] The target mesh

size $\overline{h}_i$ is given by

$$\overline{h}_i = h_i \left(\frac{||e_i||}{||\overline{e}||} \right)^{-1/p}. \tag{9}$$

This yields a size specification map $\overline{h}(x)$ given by

$$\overline{h}(x) = \overline{h}_i(x), \forall x \in [x_i, x_{i+1}[,$$

which can be used as a metric field:

$$L = \int_\Omega \sqrt{dx\, \overline{h}^{-2} dx} = \int_\Omega \overline{h}^{-1} dx \tag{10}$$

where L is the mesh size in the metric field associated to $\overline{h}$. If all goes well, $L \approx N$. The metric field can be scaled so as to take into account discrepancies.

The position of the nodes x_i of the new mesh are at the integer values of L, i.e. for $i = 0, 1, 2, ..., L$

$$\text{find } x_i \text{ s. t. } \int_0^{x_i} \overline{h}^{-1}\, dx = i. \tag{11}$$

4.2. Two-Dimensional Problems

For two-dimensional problems, the mesh adaptation strategy becomes more sophisticated. For an isotropic mesh, only one condition is needed, i.e. the local target mesh length $\overline{h}$. The local error indicator $||e_i||$ is computed on each vertex, and linearly interpolated. The target length $\overline{h}_i$ is then set to $c||e_i||^{-p}$, where p is the order of convergence rate, and c is a user define parameter to control global mesh coarseness. This parameter determines the level where the error indicator is to be equidistributed, and it defines a size map which is used by the unstructured mesh optimizer **OO**$\mathcal{RT}$ developed at CERCA[2].

The mesh optimizer **OO**$\mathcal{RT}$ can handle local target mesh stretching to perform anisotropic mesh adaptation. However, in this study, we only consider isotropic adaptation, so the aspect ratio target is set to one everywhere. The optimizer performs successive local mesh improvements to minimize a cost function used to measure the discrepancy between actual edge lengths and local target mesh lengths.

5. Numerical Examples

5.1. One-Dimensional Tests

Consider a steady quasi-one-dimensional Euler system governing compressible flows in a duct of variable cross-section

$$u_t + [f(u)]_x = s, \tag{12}$$

[2]See `http://www.cerca.umontreal.ca/oort`.

in which

$$u = \mathcal{D} \begin{pmatrix} \rho \\ \rho v \\ \rho e \end{pmatrix}, \quad f(u) = \mathcal{D} \begin{pmatrix} \rho v \\ \rho v^2 + p \\ \rho v e + v p \end{pmatrix},$$

$$s = \begin{pmatrix} 0 \\ p \frac{\partial \mathcal{D}}{\partial x} \\ 0 \end{pmatrix}.$$

For the quasi-one-dimensional problem, closed form solutions can be calculated when the area function $\mathcal{D}(x)$ is known.[21]

The following geometry has been used and its corresponding area function is given by

$$\mathcal{D}(x) = \begin{cases} d_1 & 0.0 \le x \le 0.5 \\ d_1 - k(x - 0.5)^2 & 0.5 < x \le 1.5 \\ 9/4 - 2\text{atan}(4x - 10)/3 & 1.5 < x \le 3.0 \\ a(x-2) + b/(x-2) & 3.0 < x \le 6.0 \\ d_2 + d_3[1 - (x-7)^2] & 6.0 < x \le 7.0 \\ d_2 + d_3 & 7.0 < x \le 8.0 \end{cases}$$

where $k = 4/51$, $a = 9/8 - 4/15 - \text{atan}(2)/3$, $b = 9/8 + 4/15 - \text{atan}(2)/3$, $d_1 = 9/4 + k - 2\text{atan}(-4)/3$, $d_2 = 4a + b/4$ and $d_3 = (a - b/16)/2$ are constants. To reduce the effect of boundary condition treatment, the nozzle is extended at both ends by a length of constant cross-section duct. The geometry of the nozzle is shown in Fig. 1.

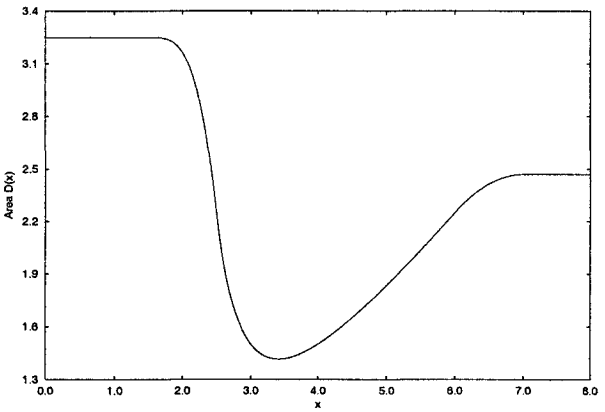

Fig. 1: Cross-section area for the nozzle.

A finite volume explicit time-marching scheme is used to solve the quasi-one-dimensional Euler Eqs. (12). The interface flux are computed using a modified Roe characteristic upwind flux-difference-splitting scheme to treat the source term more accurately.[22] With those modifications, the scheme is second-order accurate for steady state solutions over smooth flow regions. For details about the scheme and modifications, one is referred to Roe.[22]

5.2. One-Dimensional Subsonic Case

We consider first a shockless subsonic flow. At the inlet, the pressure is extrapolated from the first element value while other variables are computed using isentropic flow conditions. At the outflow boundary, the normalized back pressure is set to $p = 0.93$ and the velocity and the temperature are extrapolated from the last element.

The adaptive procedure consists in fixing the total number of vertices and trying to equidistribute the residual or the solution error. The adapted mesh spacing distributions, corresponding to the adaptations based on residual and error respectively, are compared in Fig. 2. From this figure, one can see that the refinement locations are slightly different.

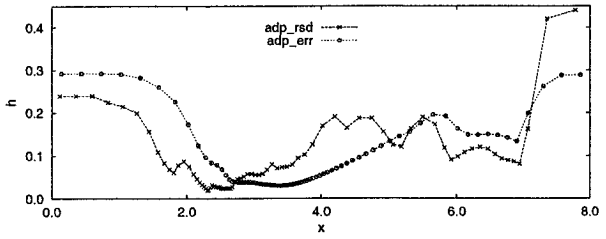

Fig. 2: Adapted mesh spacing for error indicators of residual and solution error, subsonic case.

By choosing different total number of elements N (40, 80, 160 and 320), the performance of the two error indicators has been verified. The global error and residual are plotted in Figs. 3 and 4 to show their ability to control both the error and residual. It seems that the residual based mesh adaptation is more efficient than the error based one in controlling both the solution error and the residual.

In Fig. 5, the density distribution computed with 40 elemets is shown. It can be observed that, when the mesh is relatively coarse, the difference between the two error indicators is not significant. However, as the mesh is refined, the difference becomes more and more evident. The order of convergence of adapted solutions based on the residual is almost the same as that for uniform meshes, but with an order of magnitude smaller in absolute values for both the error and the residual. However, the mesh adaptation based on solution error exhibits a tendency to reduce one efficiency index and even becomes less efficient than using uniform meshes as the number of elements is increased. This is an indication that the use of solution error to guide the mesh adaptation may work for coarse mesh but it might be a poor

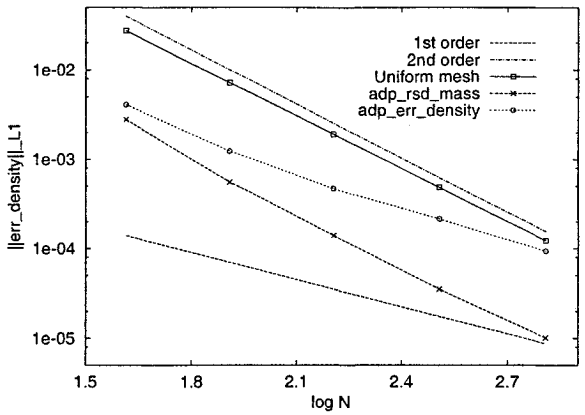

Fig. 3: Global error in function of the number of elements N, subsonic case.

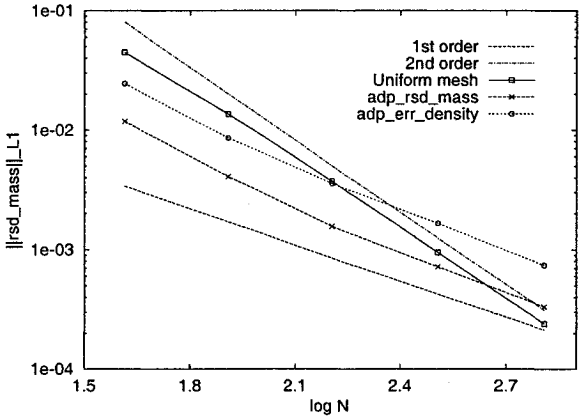

Fig. 4: Global residual in function of the number of elements N, subsonic case.

choice when the mesh becomes sufficiently fine.

5.3. One-Dimensional Transonic Case

The second test is for a transonic nozzle with a shock downstream of the throat. The shock is set at $x = 5.2$ when the back pressure is specified as $p = 0.75$. The inlet pressure is extrapolated from the first element and other properties are computed from isentropic relations. At the outlet, the velocity and the temperature are extrapolated.

The initial mesh has 40 elements with uniform spacing. As shown in Zhang *et al*,[5] for a transonic flow with a shock, the convergence rate for the error in density is only first-order in the L_1-norm and 0^{th} order for the residual for a transonic flow with a shock. In order to use the residual as an adaptive indicator, we multiply the residual by the local mesh size h which results in a first-order convergence rate in L_1-norm. In this case, the value of order as given in Eq. (9) is set to $p = 1$.

The adapted mesh spacing distributions with 132

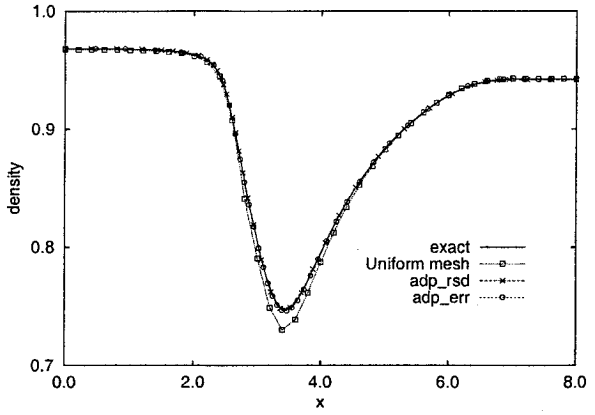

Fig. 5: Comparison of density distributions with $N = 40$, subsonic case.

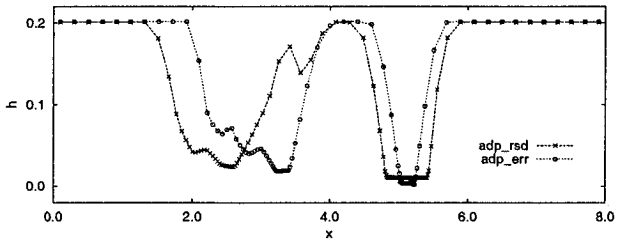

Fig. 6: Adapted mesh spacing for error indicators of residual and solution error, transonic case.

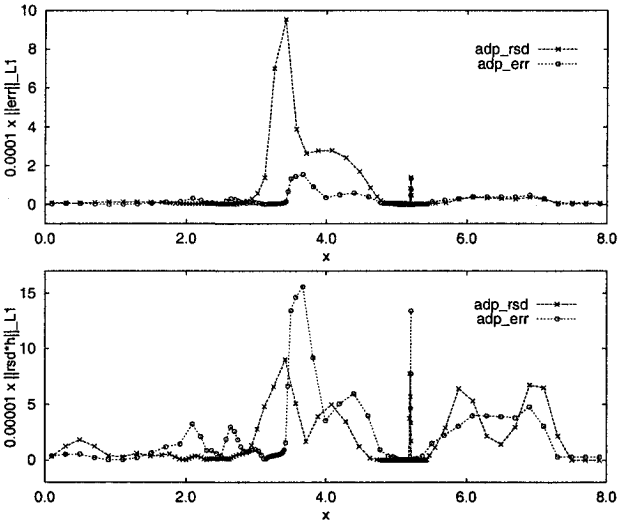

Fig. 7: Error and residual distributions for the adapted meshes, transonic case.

and 136 elements, corresponding to the adaptations based on residual and error respectively, are compared in Fig. 6. The most significant difference between these two distributions is around the sonic point ($x = 3.45$), where the solution error is relatively large but the residual is relatively small. As a result, the solution error around the sonic point has been amplified when the mesh is adapted

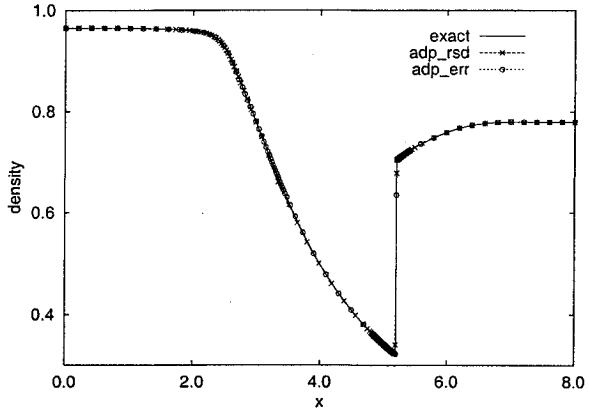

Fig. 8: Comparison of density distributions, transonic case.

with residual indicator as demonstrated in Fig. 7 even if the residual has been well controlled. This is attributed to the fact that the error occurring around the sonic point (entropy violation even with the Harten's correction[23]) is dominated by the locally created error and is weakly related to the transported error. It seems that the use of residual-based indicator is not effective for the sonic point. Both adapted meshes produce reasonably good density profiles as shown in Fig. 8, especially across the shock. It is also observed that there is a little discrepancy around the sonic point with the adapted mesh using the residual indicator.

5.4. Two-Dimensional Tests

The study is now extended to two-dimensional cases. The two-dimensional Euler equations are solved using the HURRICANE flow solver developed at UTIAS.

5.5. Two-Dimensional Subsonic Case

An inviscid subsonic flow over a NACA0012 profile has been investigated first. The initial mesh is an unstructured triangular mesh with vertices concentrated near the airfoil which results in a total of 4212 triangles and 2203 vertices (see Fig. 9). The free stream Mach number is 0.63 and the angle of attack is 2.0 degrees.

In order to compute the true error $\text{Err} = \|\rho - \rho_h\|$, a reference solution has been computed on a very fine (more than 40000 vertices) adapted mesh. The density contours of this reference solution are depicted in Fig. 10, which shows no shock wave, but two singularities at trailing edge and at the stagnation point.

Computed density contours for the initial coarse mesh are shown in Fig. 11. Error and residual distributions are compared in Fig. 12. From this figure, one can see that the locations of large residual and errors are slightly different.

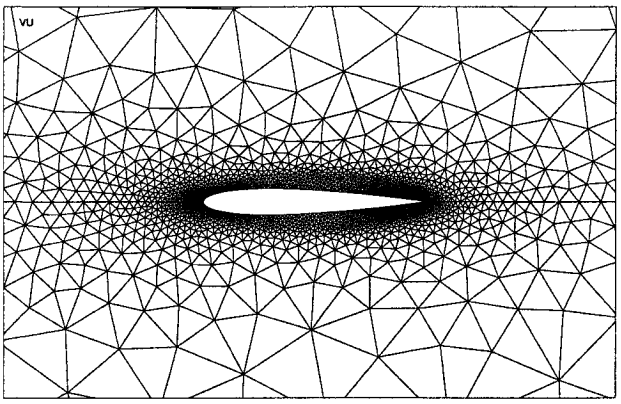

Fig. 9: Initial mesh used for subsonic and transonic two-dimensional cases. A family of finer meshes is created using the same relative vertex spacing distribution.

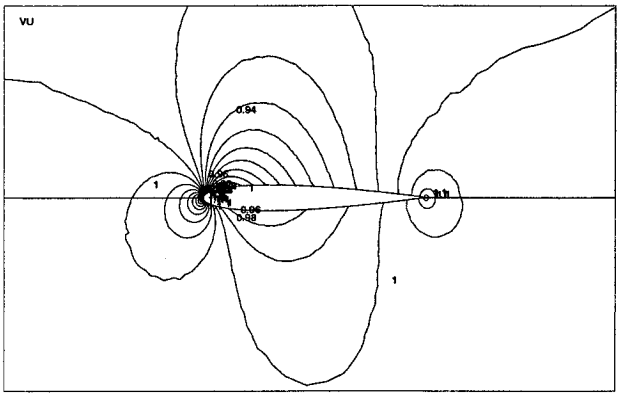

Fig. 10: Density field of the reference solution for the two-dimensional subsonic case.

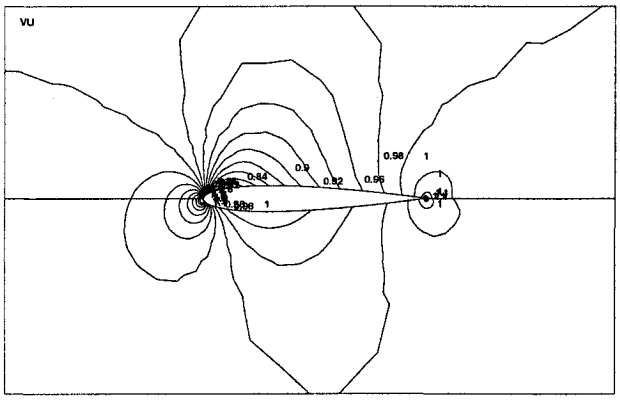

Fig. 11: Computed density on the initial mesh, subsonic case.

First of all, the convergence rate of the numerical method is measured on a family of meshes having the same relative vertex spacing distribution as the initial one (see Fig. 9). Global $L_1(\Omega)$-norm of the error is plotted in function of the number of vertices on Fig. 14 (curve labeled as "`Uniform mesh`"). It is established that the method is first order in both L_1- and L_2-norms of the error $\mathrm{Err} = \|\rho - \rho_h\|$. More precisely, the convergence rate is 0.94 in L_1-norm and 0.99 in L_2-norm, from error evaluation on the two finest meshes of that family having respectively 8546 and 33945 vertices. In terms of residual, the convergence rate is only $3/4$ in L_1-norm (0.77 from the two finest computations).

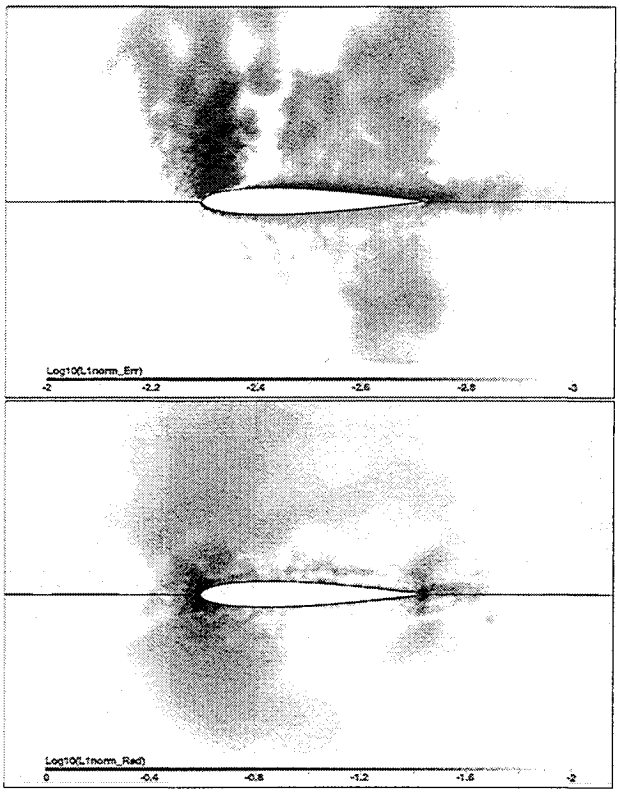

Fig. 12: Error distribution (top) and residual distribution (bottom) on the initial mesh, subsonic case.

An error indicator based on the Hessian matrix of the density is obtained from solution reconstruction and used to guide mesh adaptation. The mesh after two cycles of adaptation is shown in Fig. 13 (top). The mesh has a total of 8847 triangles and 4558 vertices which are more concentrated around both ends of the profile.

A new error indicator has also been tried to guide the mesh adaptation. It is related to the residual of the mass equation of steady state Euler Eqs. (1)

$$\mathrm{Rsd} = \nabla \cdot (\rho u, \rho v)\,.$$

The indicator involves second derivatives of ρu in x-direction and of ρv in y-direction. Derivatives are obtained from solution reconstruction. It is not an indicator of the residual error, as was the case for the one-dimensional problem. It's another error indicator of solution error which is related to the residual of the PDE. The hope is that this indicator will account for some of the transport of the error. The resulting adapted mesh after two cycles of adaptation is plotted in Fig. 13 (bottom)

for comparison. The mesh has a total of 7972 triangles and 4110 vertices.

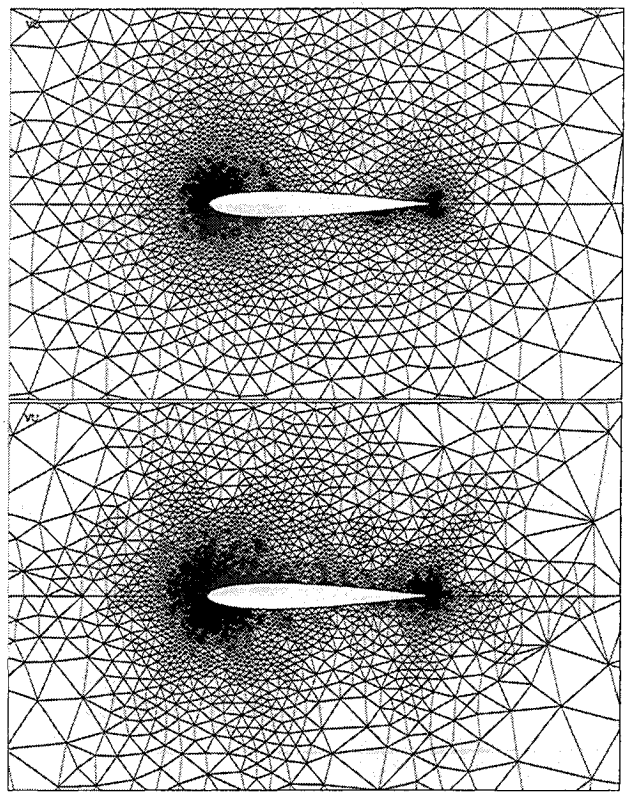

Fig. 13: Third adapted meshes in both adaptation strategies for subsonic case. Top: adaptation driven by Hessian of density; bottom: adaptation on the error indicator related to the residual of the mass equation.

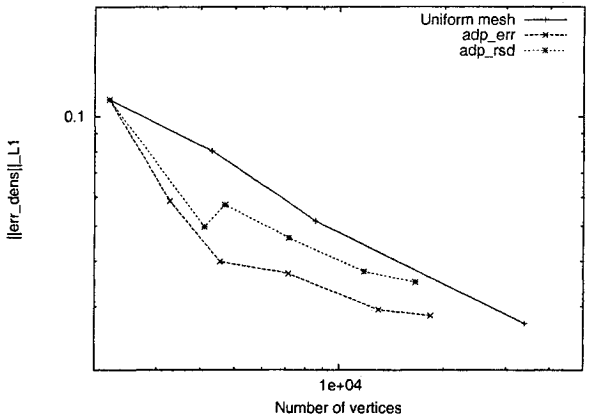

Fig. 14: Global error on the density in L_1-norm in function of the number of vertices, subsonic case.

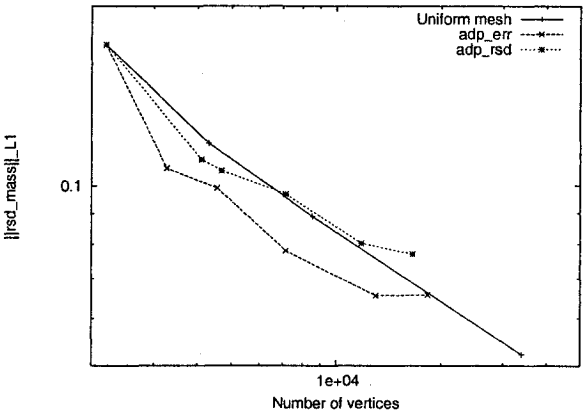

Fig. 15: Global residual in L_1-norm in function of the number of vertices, subsonic case.

The order of the method has been set to $p = 1$ in evaluating the target mesh size for both indicators. The performance of the two error indicators has been verified in function of the number of vertices. The global error and residual are plotted in Figs. 14 and 15 to show their ability to control the error and residual. It seems that the error based mesh adaptation is more efficient than the residual based one in controlling both the solution error and residual. Both adaptation strategies have nearly the same behavior: when the mesh is relatively coarse, the order of convergence is almost the same as that found with uniform refinement of the initial mesh. However, some performance degradation is observed. That is similar to the behavior of the error indicator of the solution error studied in the one-dimensional subsonic case.

5.6. Two-Dimensional Transonic Case

The last test is for transonic inviscid flow over a NACA0012 airfoil at a Mach number of 0.80 and at 1.25 degree angle of attack. The solution has two attached shocks, a strong one on the suction side and a very weak one on the pressure side. The initial mesh is the same as the subsonic case initial mesh.

A reference solution has been computed on a very fine stretched adapted mesh. The weak shock does not appear on the reference density contours (see Fig. 16 (top)). However, it has been captured in this reference solution. In fact, it appears in the error distribution $\mathrm{Err} = \|\rho - \rho_h\|$ on Fig. 17 (top), where ρ is the reference density and ρ_h is the density of solution over initial mesh.

It can be observed in Fig. 17 that the error and residual distributions have different distributions. The error distribution is concentrated upstream and downstream the two shocks. The residual distribution is nearly symmetrical and concentrated near the leading and trailing edges. The strong shock is barely detected by the residual estimate, due to the fact that the shock can not be computed on such a coarse mesh.

Starting from the computed solution over the initial mesh, the two adaptation strategies are applied to obtain finer adapted meshes. They are guided by the same error

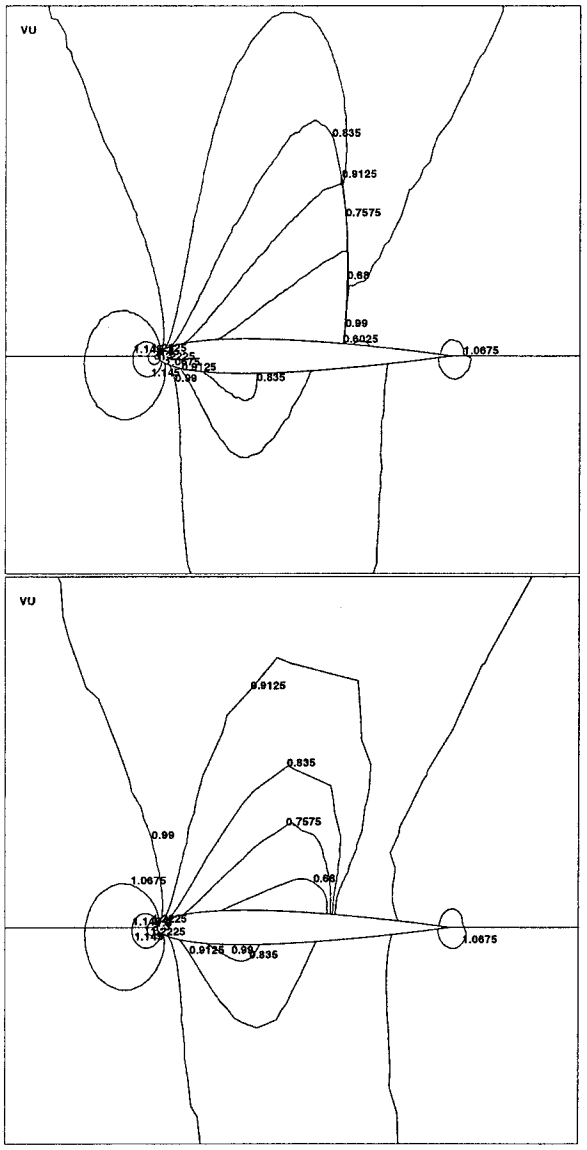

Fig. 16: Density field of the reference solution, and computed density on the initial mesh, transonic case.

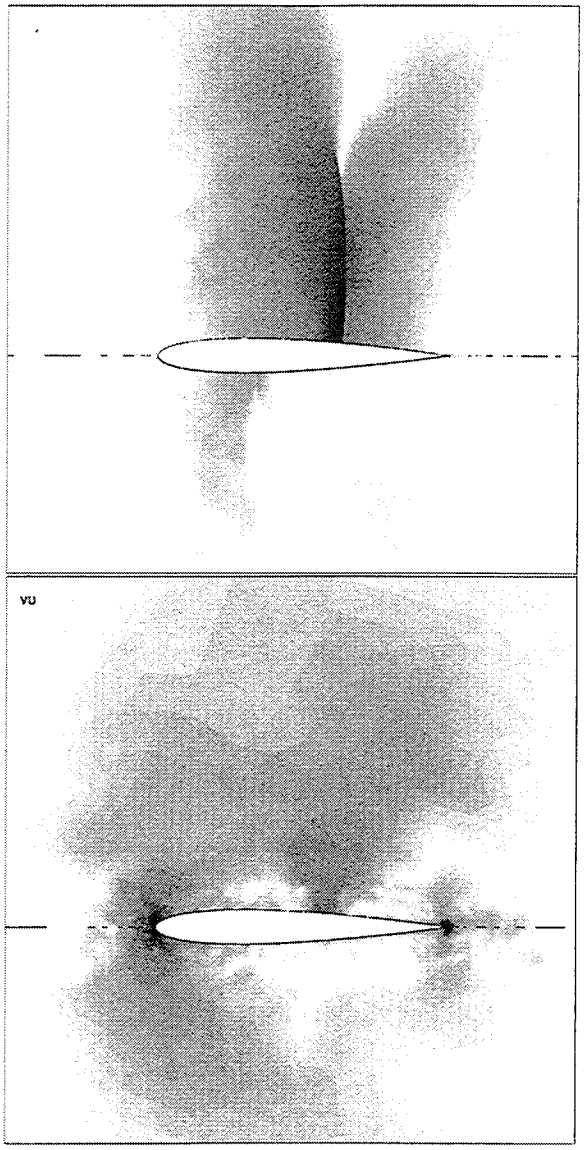

Fig. 17: Error (top) and residual (bottom) distributions on the initial mesh, transonic case.

indicators as for the subsonic case. The second adapted mesh using both strategies are shown in Fig. 18.

The meshes are clustered near the leading and trailing edges and around the shock. In fact the mesh spacing appears to have a pattern similar to that of the residual. They do not look like the error distribution. This is likely due to the fact that both indicators are based on solution reconstruction. The additional information about the PDE that is built in the error indicator based on the residual is not adequate to account for the transport of the error.

Adaptation guided by the error indicator based on solution error leads to smoother meshes. Furthermore, it seems to control the error distribution better than the adaptation guided by the new error indicator (see Fig. 19).

6. Conclusions

We have discussed two types of error indicators for mesh adaptation to control the error in the solution of the Euler equations. Numerical tests with subsonic and transonic flows have been conducted and presented for one-dimensional and two-dimensional test cases.

For one-dimensional subsonic flow, numerical test shows that the solution error indicator and the residual error indicator are efficient to control both the error and the residual over relatively coarse meshes. When the meshes become sufficiently fine, however, the residual error in-

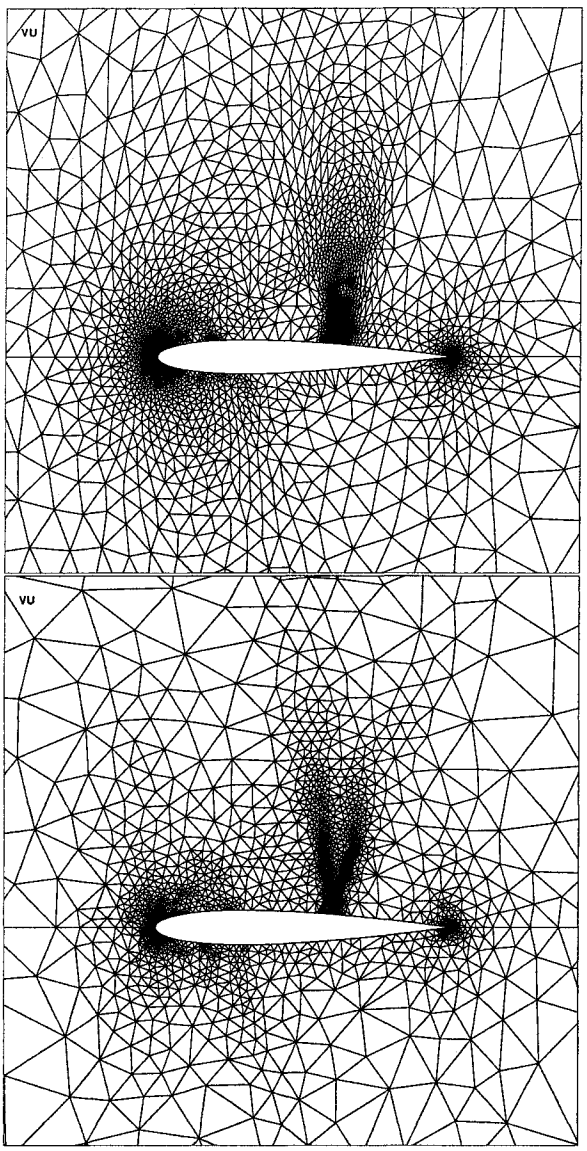

Fig. 18: Adapted meshes for error indicator of solution error (top), and error indicator related to the residual of the mass equation (bottom), transonic case.

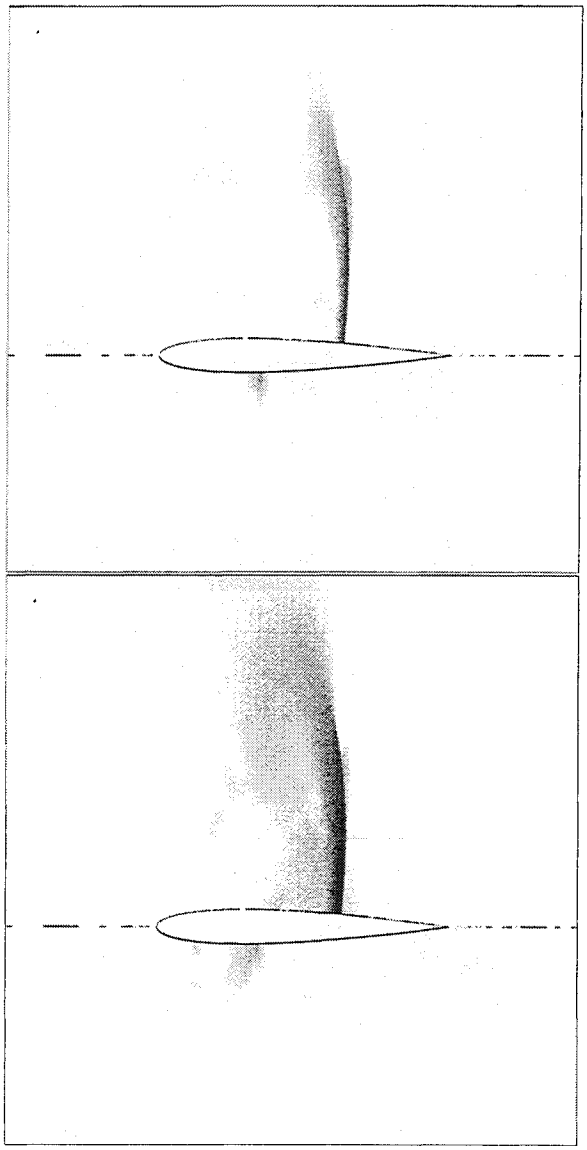

Fig. 19: Error distribution on adapted meshes using different error indicators. Top: solution error; bottom: residual of the mass equation.

dicator appears more efficient.

When transonic flow with shocks is considered, adaptation based on residual error accounts for the transported error. Refinement occurs at the location of the source error rather than where the error manifests itself. The weak point is that the residual based indicator is not effective for the sonic point, where the error is dominated by the locally created error.

The extension of previous one-dimensional results to two-dimensional cases is not obvious. For subsonic flows, the convergence rate of the scheme is first-order in the L_1-norm of the error in density. The mesh adaptation strategy is to equidistribute the error indicator. Some results can be extended from one to two dimensions. The location of error and residual peaks differs for transonic and subsonic cases; the behavior of the global error as well as the global residual during mesh adaptation driven by a solution error indicator is comparable for subsonic cases. Further work is required to develop an effective residual error estimator for the two-dimensional Euler equations.

Acknowledgments

This work was financially supported by Bombardier Aerospace and NSERC of Canada.

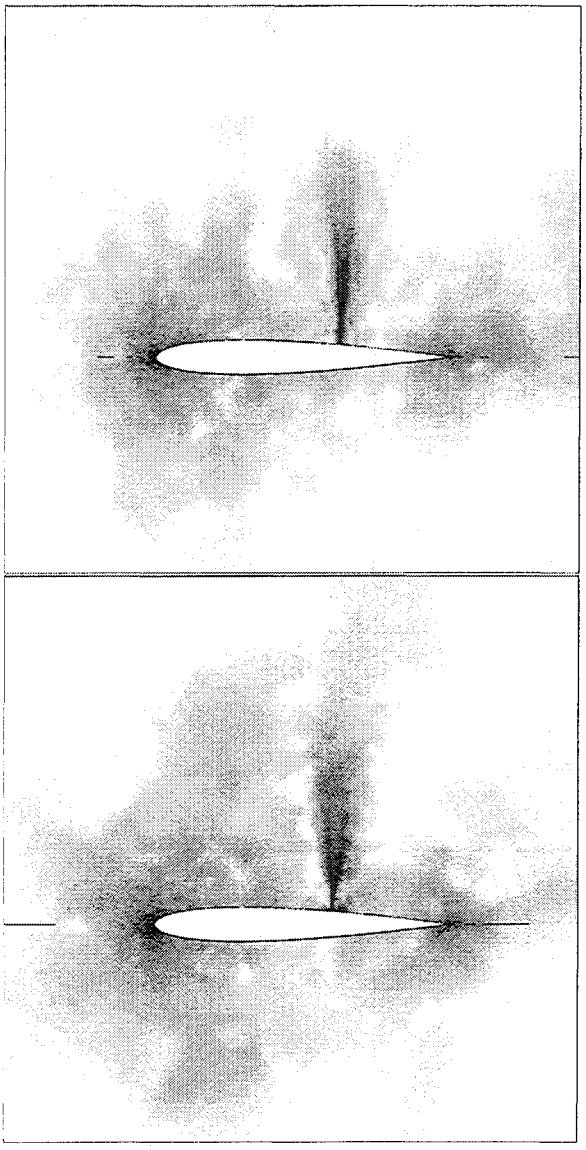

Fig. 20: Residual distribution on adapted meshes using different error indicators. Top: solution error; bottom: residual of the mass equation.

References

[1] O. C. Zienkiewicz and J. Z. Zhu. A simple error estimator and adaptive procedure for practical engineering analysis. *Int. J. Numer. Meth. Eng.*, 24:337–357, 1987.

[2] O. C. Zienkiewicz and J. Z. Zhu. The superconvergent patch recovery and a posteriori error estimates. Part 1: the recovery techniques. *Int. J. Numer. Meth. Eng.*, 33:1331–1364, 1992.

[3] P. J. Roache. *Verification and Validation in Computational Science and Engineering*. Hermosa Publishers, Albuquerque, New Mexico, USA, 1998.

[4] X. D. Zhang, J.-Y. Trépanier, and R. Camarero. A posteriori error estimation method for finite-volume solutions of hyperbolic conservation laws. *Computer Method in Applied Mechanics and Engineering*, 185(1):1–19, April 2000.

[5] X. D. Zhang, D. Pelletier, J.-Y. Trépanier, and R. Camarero. Verification of error estimators for the Euler equations. In *The AIAA 38th Aerospace Science Meeting & Exhibit*, 2000. AIAA Paper 2000–1001, January 10–13, Reno, USA.

[6] X. D. Zhang, D. Pelletier, J.-Y. Trépanier, and R. Camarero. Error estimation and control for the Euler equations. In *Fluids 2000*, 2000. AIAA Paper 2000–2246, June 19–22, Denver, USA.

[7] X. D. Zhang, D. Pelletier, J.-Y. Trépanier, and R. Camarero. Error control and mesh adaptation for the Euler equations. In *The AIAA 39th Aerospace Science Meeting & Exhibit*, 2001. AIAA Paper 2001–0441, January 8–10, Reno, USA.

[8] T. Sonar and E. Suli. A dual graph-norm refinement indicator for finite volume approximations of the Euler equations. *Numerische Mathematik*, 78:619–658, 1998.

[9] J. V. Lassaline and D. W. Zingg. Aerodynamic computations using an agglomeration multigrid strategy with directional coarsening. In *The 46th Annual Conference of Canadian Aeronautics and Space Institute*, Montreal, May 3–5 1999.

[10] P. G. Ciarlet. *The finite element method for elliptic problems*. North-Holland Publishing Company, Amsterdam, 1978.

[11] K. W. Morton and E. Suli. A posteriori and a priori error analysis of finite volume methods. In *The Mathematics of Finite Elements and Applications*. John Wiley & Sons Ltd, 1994. Chapter 18, Edited by J. R. Whiteman.

[12] J. A. Peraire, M. Vahdati, K. Morgan, and O. C. Zienkiewicz. Adaptive remeshing for compressible flow computations. *Journal of Computational Physics*, 72:449–466, 1987.

[13] C. Ilinca, X. D. Zhang, J.-Y. Trépanier, and R. Camarero. A comparison of three error estimation techniques for finite-volume solutions of compressible flows. *Computer Method in Applied Mechanics and Engineering, (in print)*, 189(4):1277–1294, October 2000.

[14] M.-G. Vallet. *Génération de maillages éléments finis anisotropes et adaptatifs*. PhD thesis, Université Pierre et Marie Curie, Paris VI, France, 1992.

[15] P.-L. George and H. Borouchaki. *Triangulation de Delaunay et Maillage*. Hermès, Paris, 1997.

[16] I. Babuška and W. C. Rheinboldt. Error estimates for adaptive finite element computations. *SIAM Journal of Numerical Analysis*, 15(4):736–754, 1978.

[17] T. Sonar. Strong and weak norm refinement indicator based on the finite element residual for compressible flow computations. *Impact of Comp. in Sci. and Eng.*, 5:111–127, 1993.

[18] J. A Mackenzie, T. Sonar, and E. Suli. Adaptive finite volume methods for hyperbolic problems. In *The Mathematics of Finite Elements and Applications*. John Wiley & Sons Ltd, 1994. Chapter 19, Edited by J. R. Whiteman.

[19] T. Sonar, V. Hannemann, and D. Hempel. Dynamic adaptivity and residual control in unsteady compressible flow computation. *Mathematical and Computer Modelling*, 20(10/11):201–213, 1994.

[20] O. C. Zienkiewicz and R. L. Taylor. *The finite element method, Vol. 1*. McGraw-Hill Book Company, London, fourth edition, 1989.

[21] F. M. White. *Fluid Mechanics*. McGraw-Hill, Third edition, 1994.

[22] P. L. Roe. Characteristic-based schemes for the Euler equations. *Annual review of fluid mechanics*, 18:337–365, 1986.

[23] A. Harten. High resolution schemes for hyperbolic conservation laws. *J. Comp. Phys.*, 49:357–393, 1983.